Elsevier Editorial System(tm) for Journal of Wind Engineering & Industrial Aerodynamics

Manuscript Draft

Manuscript Number:

Title: Spectral Coherence Model for Power Fluctuations in a Wind Farm

Article Type: Full Length Article

Keywords: wind models; wind coherence; power fluctuation; offshore wind farms

Corresponding Author: Antonio Vigueras-Rodríguez, PhD student, Industrial Engineer.

Corresponding Author's Institution: Universidad Politécnica de Cartagena

First Author: Antonio Vigueras-Rodríguez

Order of Authors: Antonio Vigueras-Rodríguez; Poul E Sørensen, Senior Scientist, M.Sc. in Electrical Engineering.; Antonio Viedma Robles, Professor, Aeronautical Engineer.; Martin H Donovan, M.Sc. in Energy Engineering

Manuscript

Spectral Coherence Model for Power Fluctuations in a Wind Farm

A. Vigueras-Rodríguez [a,*],P. Sørensen [b], A. Viedma [a]
M. H. Donovan [c]

[a] *Thermal and Fluids Egineering Department, Universidad Politécnica de Cartagena. Cartagena, Murcia, Spain.*

[b] *Wind Energy Department, Risø DTU, Roskilde, Denmark*

[c] *DONG Energy, Copenhagen, Denmark*

Abstract

This paper provides a model for the coherence between wind speeds located in a horizontal plane corresponding to hub height of wind turbines in a large wind farm.

The model has been developed using wind speed and power measurements from the 72 Wind Turbines and 2 of the meteorological masts from Nysted Offshore Wind Farm during 9 months.

The coherence model developed in this paper is intended for use of power fluctuations in large offshore wind farms. In this way, analysing the current coherence models it is shown the needing of a new one, adapted to the characteristic distances and the related time scale.

Key words: wind models, wind coherence, power fluctuation, offshore wind farms
PACS: 89.30.Ee

1 Introduction

Nowadays the concern about the effects of the pollution (like the global warming effect) and the knowledge of the limitations of the fossil resources are creating a strong tendency in Europe towards the use of renewable energy sources. Therefore, there has been a big growth in the Wind Energy development, and it is expected to go on rising. Such growth makes essential to research deeply

* Corresponding author.
Email address: avigueras.rodriguez@upct.es (A. Vigueras-Rodríguez).

into this energy technology from the point of view of an important component of the electrical system, instead of considering only the local voltage quality as it was done previously (Sørensen et al., 2007).

A major issue in the control and stability of electric power systems is to maintain the balance between generated and consumed power. Because of the fluctuating nature of wind speeds, the increasing use of wind turbines for power generation has risen the interest in the fluctuations of the wind turbines power production, especially when the wind turbines are concentrated geographically in large wind farms. That fluctuation can also be a security issue in the future for systems with weak interconnections like Ireland or the Iberian Peninsula.

As example of the significance of these power fluctuations in Energinet.dk (the Danish Transmission System Operator), according to Akhmatov et al. (2004), Energinet.dk has observed that power fluctuations from the 160 MW offshore wind farm Horns Rev in West Denmark introduce several challenges to reliable operation of the power system in West Denmark. And also, that it contributes to deviations from the planned power exchange with the Central European Power System (UCTE). Moreover, it was observed that the time scale of the power fluctuations was from tens of minutes to several hours.

And in those fluctuations the importance of the spatial correlation of the wind speed in that time frame is shown by the fact that the power fluctuations of the 160 MW Wind Farm was significantly greater than the fluctuations in a similar capacity of Wind Turbines (WTs) distributed in smaller onshore Wind Farms. Those conclusions point out that the research of the spatial correlation is a main topic for the power fluctuation analysis.

In this way, models of coherence have been used within the modelling of wind farms regarding power fluctuation. Sørensen et al. (2002) developed a wind speed model for a wind farm using a coherence model. In this case, the aim of the model was to simulate the fluctuations in the shorter time scales related with the power quality characteristics.

Later on, an overall model for power fluctuations regarding the "long term" fluctuations described above has been developed (Sørensen et al., to appear).

2 Coherence models for Power Fluctuation

The spectral coherence between the wind speed in two different points is defined by

$$\gamma(f) = \frac{S_{ab}(f)}{\sqrt{S_{aa}(f)S_{bb}(f)}} \tag{1}$$

where $S_{ab}(f)$ is the crossed power spectral density (CPSD) between the wind speed in points a and b, and $S_{aa}(f)$ and $S_{bb}(f)$ are the power spectral density (PSD) of the wind in each point.

Besides the practical observation of the link between the power fluctuation and the spectral coherence above cited, different theoretical and practical observations have appeared in recent papers (Nanahara et al., 2004; Sørensen et al., to appear) confirming that the seeking of power fluctuations models is totally linked with the coherence models in a wind farm frame.

Regarding the current coherence models, most of them are based in modifications to the Davenport model (Davenport, 1961). Davenport's model suggest an exponential behaviour explained by the following expression

$$|\gamma| = e^{-a\frac{d\cdot f}{V}} \tag{2}$$

where a, that is usually called decay factor, is a constant.

This model does not explain the inflow angle dependence, and so the usual modifications of this model, based in changing the value of the constant a or even in suggesting a stochastic behaviour for it (Solari, 1987), have the same problem when using them in the scale of a wind farm, where this dependence is essential (Vigueras-Rodríguez et al., 2006).

Nevertheless, the modifications suggested by Schlez and Infield (1998) introduced that dependency expressing a as a function of the inflow angle

$$a = \sqrt{(a_{long}\cdot\cos\alpha)^2 + (a_{lat}\cdot\sin\alpha)^2} \tag{3}$$

being a_{long} and a_{lat} respectively the decay factors for the longitudinal and the lateral situations given by

$$a_{long} = (15 \pm 5)\cdot I_V \tag{4}$$

$$a_{lat} = (17.5 \pm 5)(m/s)^{-1}\cdot I_V\cdot\bar{V} \tag{5}$$

being I_V the turbulent intensity defined by $I_V = \frac{\sigma_v}{V}$

However, this empirical model was based on a very limited distance scale and so it does not predict the behaviour in the large wind farms of nowadays (Vigueras-Rodríguez et al., 2006), so none of the usual models used in Wind Energy suits for studying the Power Fluctuation of Wind Farms. Therefore, in this paper the spectral coherence within a large wind farm is studied, with the aim of suggesting a suitable model.

3 Experimental data used

The data used in this work is based in the Nysted Wind Farm, which is an offshore Wind Farm compound of 72 Siemens SWT-2.3-82 fixed speed wind turbines, with a global nominal power of 165.6 MW and distances between the wind turbines between 0.48 km and 7.73 km.

In the 72 WTs and the 2 Meteorological Masts shown in the figures, it has been measured the wind speed in the nacelle of each WT (69 m above ground), the active power produced, the yaw angle, the angular velocity and other variables. Furthermore, we have accesed to the wind speed and wind direction data from the meteorological masts at 70 m. above ground.

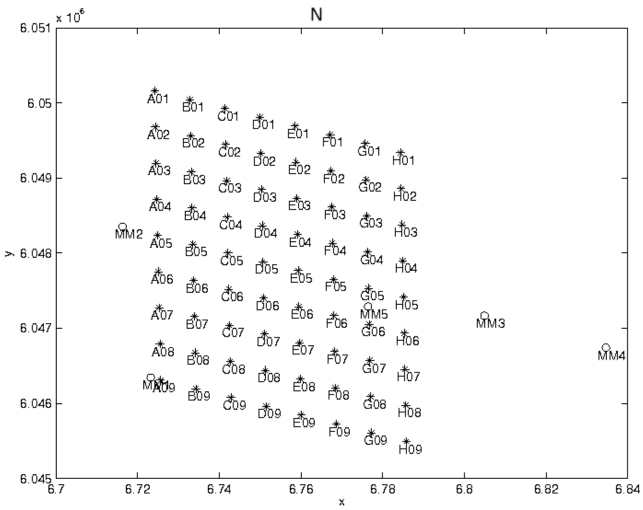

Figure 1. Layout of the Nysted Wind Farm

All of those data have been obtained through a SCADA system used by the wind farm main controller, which logs the data with a 1Hz sampling frequency.

The data stored that have been used for this work is basically the wind speeds measured by each WT and the velocity and direction of the wind measured in the masts MM2 and MM3 that are shown in the figure 1, corresponding to 9 months in 2005.

4 Procedure of the coherence measuring

For obtaining a coherence model in a suitable time frame for this purpose, 2 hour intervals have been considered. Next, it has been selected only intervals with a 75% of valid data in MM_2 and MM_3. For the single Wind Turbine data a filtering for each Wind Turbine working in a "normal" state has been done by selecting the WTs with at least a 90% of valid data and holes smaller than 3 seconds, so that they can be fulfilled using splines without having any significant influence to the time scale that we are studying.

Then, it has been define similar pairs of WTs with similar distances and angles like A_{01}-A_{02} and C_{03}-C_{04}, calling them segments.

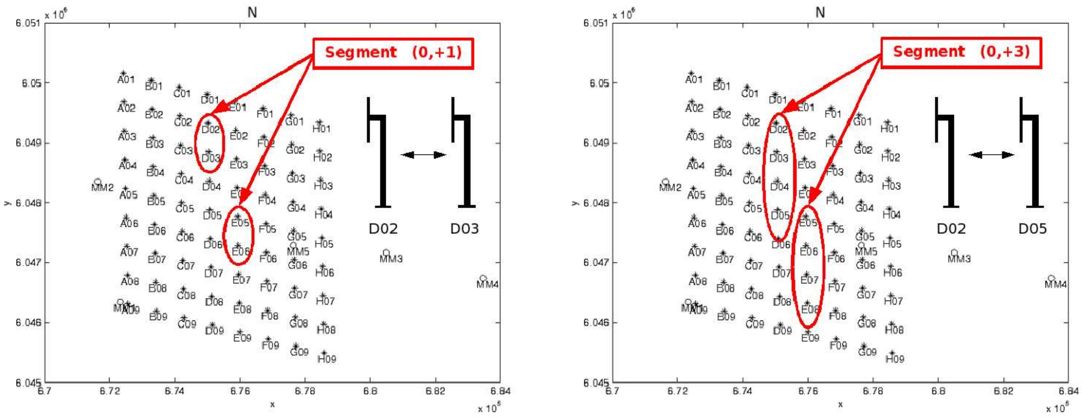

Figure 2. Example of how the segments are assembled

Following this process, as it is shown in figure 2, we consider all segments with more than 8 couples, as example some of those segments are shown in the table 1.

Once having selected the intervals, the data in each time interval are processed, averaging the power spectra of each couple of WTs belonging to the same segment.

For instance, when we consider the segment n compound of m pairs (being $m \geq 8$) of WTs with valid data (a_i, b_i), regarding the convolution property of the Fourier Transform:

$$S_{aa} = \frac{\sum_{i=1}^{m} \mathbf{FFT}(V_{a_i}) \cdot \mathbf{FFT}(V_{a_i})^*}{m} \tag{6}$$

Δi_{row}	Δi_{column}	d_{xy}(m)	β_{xy}(deg.)	Blocks
0	1	482	-2	64
0	2	964	-2	56
0	3	1445	-2	48
1	1	1062	-56	56
5	4	5041	-60	15
1	-4	1972	23	35

Table 1
Example of the 2-point segment characteristics.

$$S_{bb} = \frac{\sum_{i=1}^{m} \mathbf{FFT}(V_{b_i}) \cdot \mathbf{FFT}(V_{b_i})^*}{m} \tag{7}$$

$$S_{ab} = \frac{\sum_{i=1}^{m} \mathbf{FFT}(V_{a_i}) \cdot \mathbf{FFT}(V_{b_i}^*)}{m} \tag{8}$$

where $S_{aa}(f), S_{bb}(f) \in \mathbb{R}$, as well as $S_{ab}(f) \in \mathbb{C}$. This is done for each segment with enough valid data in each time interval.

Afterwards, the results of each segment data $(S_{aa}(f), S_{bb}(f), S_{ab}(f))$ can be classified depending on the average wind speed $\overline{V}$ and the inflow angle α calculated through the segment angle β and the wind direction ϕ as shown in figure 3.

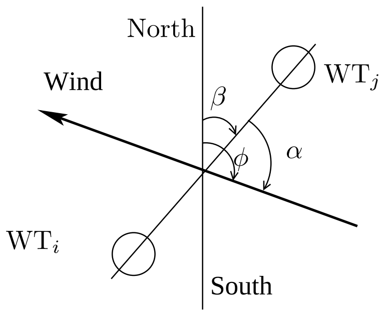

Figure 3. Definition of the inflow (α), segment (β) and wind direction angles (ϕ) used.

Next, the data classified for each segment (n) in the same wind speed range (v_m) and inflow angle range (α_k) are used for calculating the coherence $\gamma(n, v_m, \alpha_k, f)$ as follows:

$$\gamma(n, v_m, \alpha_k, f) = \frac{\sum_{i=1}^{N_n} S_{ab}(i, f) \cdot N_i}{\sqrt{\sum_{i=1}^{N_n} S_{aa}(i, f) \cdot N_i \cdot \sum_{i=1}^{N_n} S_{aa}(i, f) \cdot N_i}} \tag{9}$$

where N_i are the number of pairs of WT series of data used previously for calculating the power spectral functions, i.e. the number m in equations 6,7 and 8.

The followind 5 inflow angle bins are used $[0, 6, 25, 65, 84, 90]$(deg.), whereas the ranges of wind speed are $2m/s$ intervals from $2m/s$ to $16m/s$.

Finally, using the distance of each segment $d(n)$, we get an experimental $\gamma(d, v_m, \alpha_k, f)$.

In this proceeding the wake has been neglected, that is possible because in most of the pairs consider where both measures are inside of the overall wake, that affects similarly to both series of data and so, it is removed by the definition of the coherence itself (eq. 1). On the other hand, in the cases where the influence of having measures out of the wake and measures in the deep wake could be greater, looking at the expression of power spectral density of the wind inside and out of the wake that is shown by Sørensen et al. (to appear), we see that it does not affect to the time scale which we are interested in.

In the data considered, the average of the turbulent intensity is $\overline{I_V} = 0.12$. The turbulent intensity has not been introduced into the general analysis in order to simplify the problem, so that enough number of long distance series are available. However, hereinafter the influence of I_V is analysed using the following I_V ranges: $[0.04, 0.10]$ with an average $\overline{I_V} = 0.09$, $[0.08, 0.16]$ with $\overline{I_V} = 0.12$ and finally $[0.12, 0.20]$ with $\overline{I_V} = 0.15$.

5 Results

As it has been explained previously we have a package of coherence data $(|\gamma(d, v_m, \alpha_k, f)|$ and its argument $\angle\gamma(d, v_m, \alpha_k, f))$, from which we focus mainly in the module part.

Looking into the data, it is found a clear exponential dependence between the coherence and either the frequency f or the dimensionless frequency $fracd \cdot fV$, as it is shown in figure 4. Although looking at the exponential dependence in different situations, it is also shown that its decay factors are quite different on each situation, and therefore it is not convenient to fit it to a single decay factor.

Then, taking into account the inflow angle, we can focus firstly in the data corresponding to the longitudinal situation ($\alpha_1 \Rightarrow \alpha \in [0, 6\,\mathrm{deg}]$) plotted in figure 5, where the decay factor a (see 2) is plotted for different wind speed ranges against the distance. In that figure, it is possible to see that there is not any significant tendency in the variation of that parameter with the distance or the wind speed ($a_{long} \neq f(d, V)$). Therefore, it is possible to assume that a constant value for the longitudinal situation a_{long} (see 4) would be suitable in this distance and time frame.

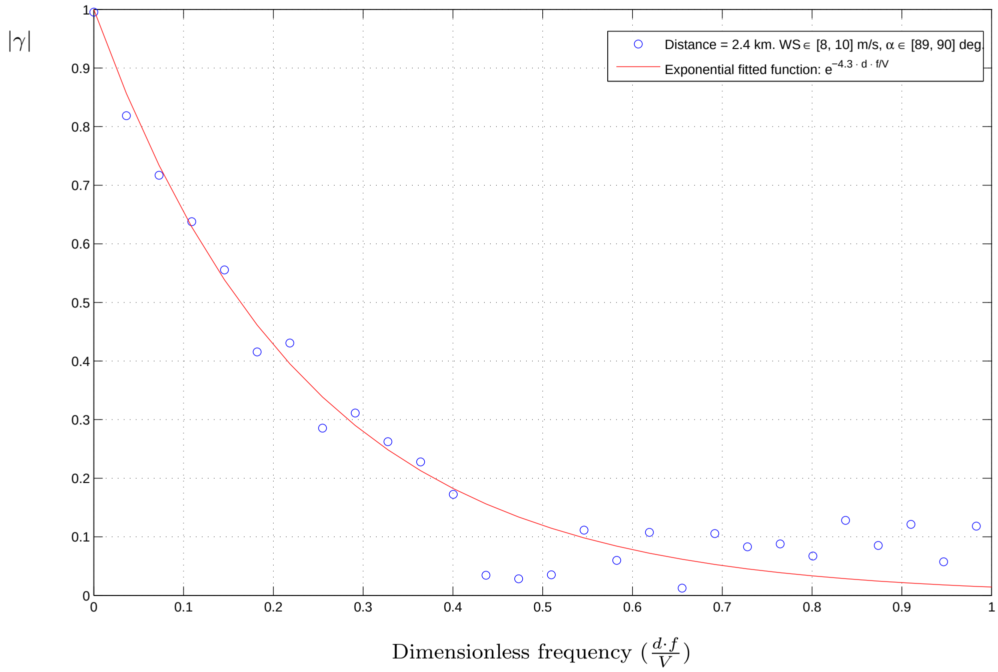

Figure 4. Coherence measured in Nysted Wind Farm in the longitudinal situation and an exponential curve fitted to the data.

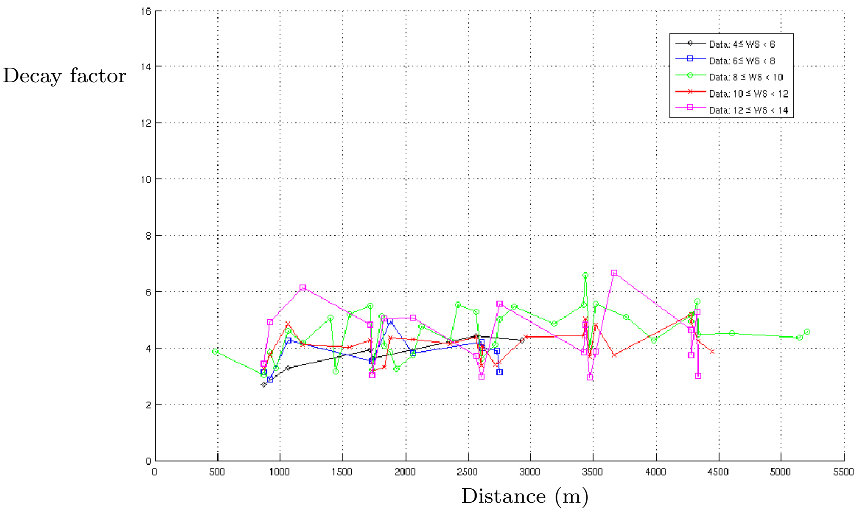

Figure 5. Decay factor of the coherence in the longitudinal situation.

However, in the lateral situation ($\alpha_5 \Rightarrow \alpha \in [84, 90\,\text{deg}]$), the decay factor parameter depends significantly on the distance and the wind speed ($a_{lat} = f(d, V)$), as it is shown in figure 6.

Looking into the figure, it is possible to see that a_{lat} gets lower when the distance rises, a_{lat} rises when wind speed gets greater, and those changes of a_{lat} get less significant as the distance gets greater.

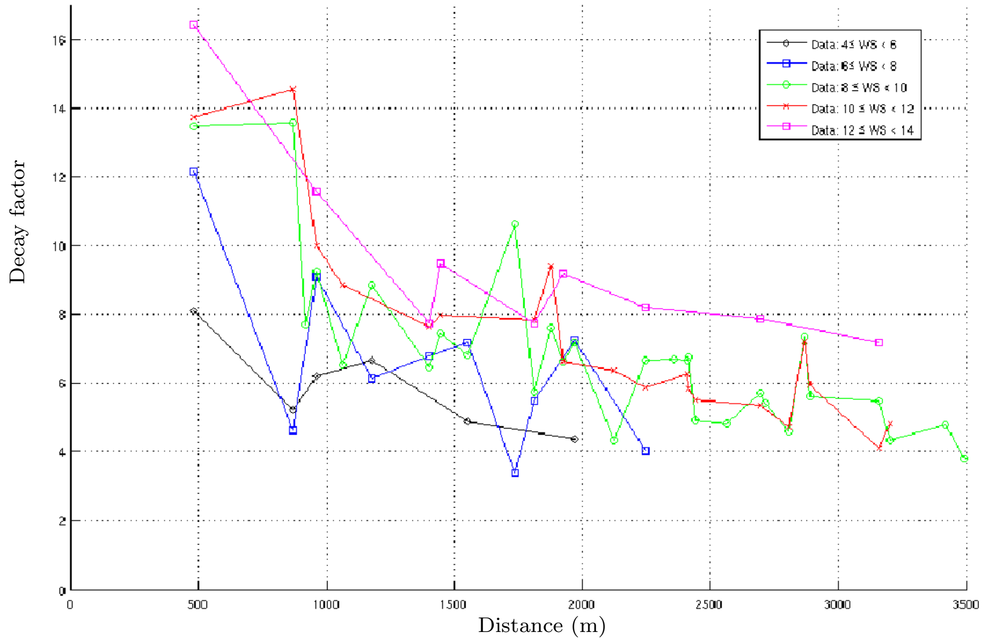

Figure 6. Decay factor of the coherence in the lateral situation.

Looking at the intermediate situations $(\alpha_2, \alpha_3, \alpha_4)$, like the one shown in figure 11 ($\alpha_4 \Rightarrow \alpha \in [65, 84\,\text{deg}]$), it is possible to see an intermediate behaviour between the longitudinal and the lateral situation, thus working with a model based on the Schlez & Infield one seems convenient.

6 Fitting of the model

Firstly, after looking the longitudinal figures shown previously in section 5, a constant value for the longitudinal decay factor (a_{long}) is introduced into the model.

The angular part of the coherence ($\angle\gamma(d, V, \alpha, f)$) is estimated through a delay time model $\tau_d = \frac{\cos(\alpha)\cdot d}{W}$, where W would be the convective velocity of the "wind wave", which in this frequency scale can be estimated by the average wind speed measured out of the wind farm $V_\infty \approx \frac{V}{0.85}$. By using the Fourier transform properties, that delay is translated into

$$\angle\gamma(d, V_\infty, \alpha, f) = e^{-2\pi f \tau_d} = e^{-2\pi f \frac{\cos(\alpha) d}{V_\infty}} \tag{10}$$

An example of comparison between above model and the experimental data can be found in figure 7.

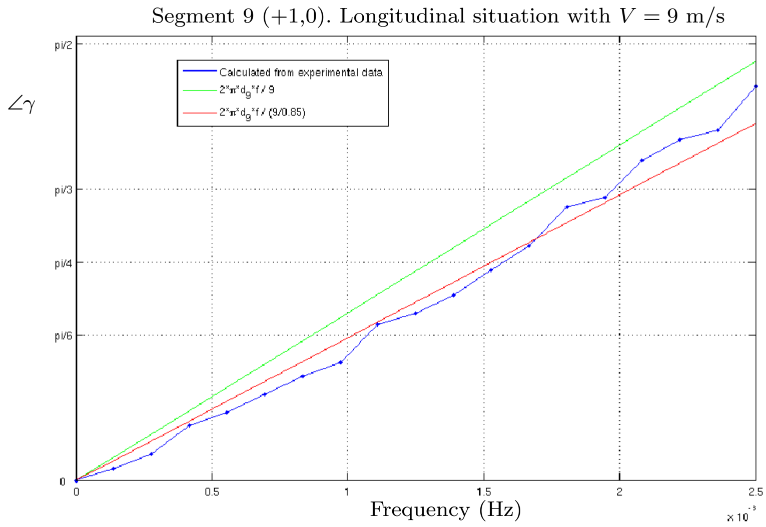

Figure 7. Comparison between the angular part of the coherence obtained from Nysted data and the delay model introduced by eq 10

Then, considering the results in the lateral situation shown in the previous section, the lateral decay factor should be modelled as a function with the following behaviour:

$$d \uparrow \Rightarrow a_{lat} \downarrow \tag{11}$$
$$V \uparrow \Rightarrow a_{lat} \uparrow \tag{12}$$
$$d \uparrow\uparrow \Rightarrow \Delta a_{lat}(\Delta d, \Delta V) \downarrow \tag{13}$$

After studying different models for the lateral decay factor, the following model has been chosen

$$a_{lat}(d, V) \approx C_1 \frac{V}{d} + C_2 \tag{14}$$

Next, the parameters of those decay factors (a_{long}, C_1, C_2) were fitted using only the data from the longitudinal and the lateral situation respectively (α_1 and α_5), this was done by minimising the error of the model when trying to estimate $\log(\gamma)$, reducing it to a linear optimisation process, in which each segment data is weighted by $N_{S_n} = \sum_i^{N_n} N_i$ (see equation 9).

Afterwards, using those values as initial point of a simplex method the model is fitted to the overall data $|\gamma(d, V, \alpha, f)|$ in all the inflow angle ranges. Arriving to the following model for the absolute value of the coherence:

$$|\gamma(d,V,\alpha,f)| = e^{\sqrt{(a_{long}\cdot\cos\alpha)^2+(a_{lat}(d,V)\cdot\sin\alpha)^2}\,\frac{d\cdot f}{V}} \tag{15}$$

$$a_{long} \approx \quad 4.5 \tag{16}$$

$$a_{lat}(d,V) \approx \quad 466(s)\frac{V}{d} + 4.2 \tag{17}$$

This model fits quite well to the original data, having a standard deviation for the coherence data previously calculated $|\gamma(d(n),V,\alpha,f)|$ in each segment n smaller than 0.06, i.e.:

$$\sigma_\gamma = \sqrt{\frac{\sum_n N_{S_n}\cdot\left(|\gamma(d(n),V,\alpha,f)| - |\hat{\gamma}(d,V,\alpha,f)|\right)^2}{\sum_n N_{S_n}}} < 0.06 \tag{18}$$

A comparison with the original coherence data in four different situations can be found in figure 8. Regarding the decay factors, some comparisons for different wind speeds, distances and inflow angles are provided in figures 9, 10 and 11, showing all of them a good agreement between the experimental data and the model.

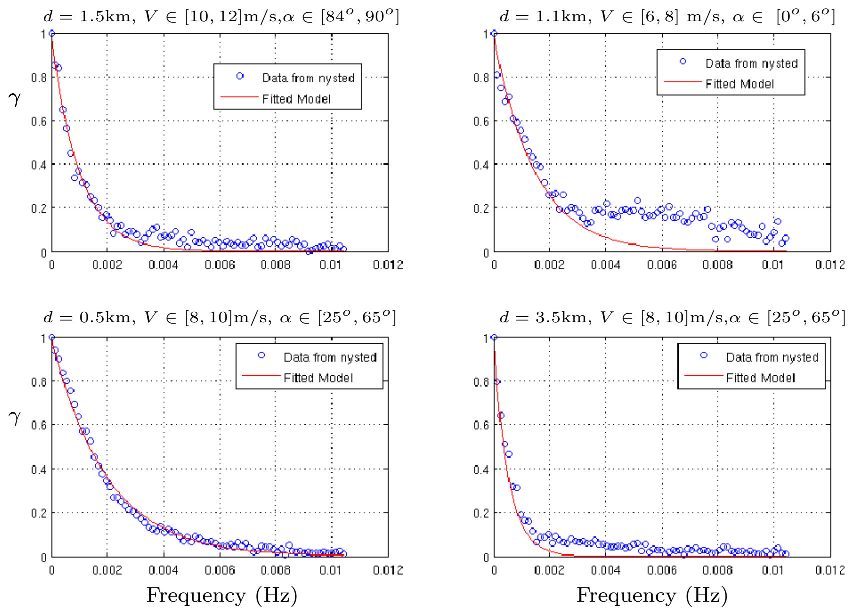

Figure 8. Comparison between the "measured" coherence and the fitted model in 4 different situations

Furthermore, as the non-dimensional constant values of the model (Eq. 15) are very closed, it is possible to simplify the model considering them equal without increasing significantly the error, so in this way we can express the coherence as follows

$$|\gamma(d,V,\alpha,f)| = e^{\sqrt{(a_{long}\cdot\cos\alpha)^2+(a_{lat}(d,V)\cdot\sin\alpha)^2}\,\frac{d\cdot f}{V}} \tag{19}$$

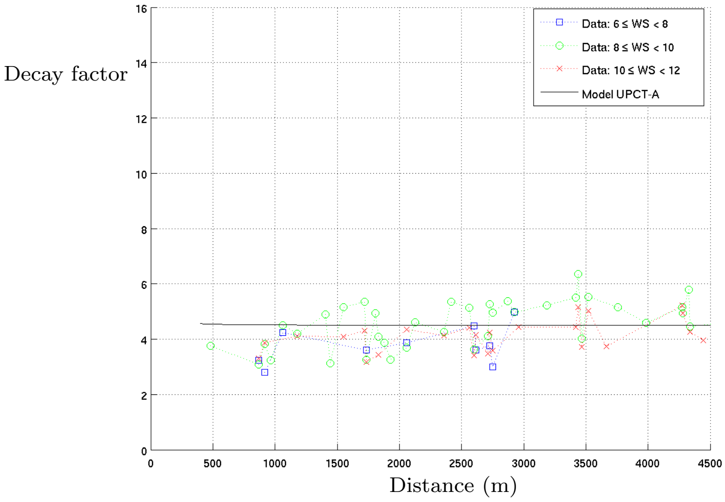

Figure 9. Comparison between the "measured" decay factors and the model proposed in this paper (UPCT-A) in the longitudinal situation.

$$a_{long} \approx \quad 4.4 \tag{20}$$

$$a_{lat}(d,V) \approx \quad 436(s)\frac{V}{d} + a_{long} \tag{21}$$

Regarding the influence of the I_V, neglected in the general proceeding as explained in section 4, in the equation 15 it does not have a considerable influence in the longitudinal term, meanwhile when I_V rises the non-dimensional term rises and the other term gets reduced proportionally to the square root of that increase. So, the influence I_V could be introduced in this way:

$$|\gamma(d,V,\alpha,f)| = e^{\sqrt{(a_{long}\cdot\cos\alpha)^2+(a_{lat}(d,V)\cdot\sin\alpha)^2}\,\frac{d\cdot f}{V}} \tag{22}$$

$$a_{long} \approx \quad 4.5 \tag{23}$$

$$a_{lat}(d,V) \approx \quad \frac{56(s)}{\sqrt{I_V}}\cdot\frac{V}{d} + 35\cdot\sqrt{I_V} \tag{24}$$

Nevertheless, its influence is not that significant and it can be neglected increasing the simplicity and not affecting to the reliability of the model. Moreover, in the simplified model (eq. 19), the influence of I_V in the lateral "time constant" is quite small.

7 Comparison to other models

The model proposed here (UPCT-A) is compared in this section with Schlez & Infield model, which is described above (eq. 3), and with the model fitted to data of the Høvsøre test station (Sørensen et al., to appear).

As we have seen the model UPCT-A as well as Høvsøre model agrees with the inflow angle dependence introduced by Schlez & Infield. And so, the longitudinal and lateral decay factors can be compared in a separate way.

The longitudinal decay factor predicted by the three models can be seen in figure 12, in which it is shown that the three models agree in suggesting a constant value for the decay factor. However, the value suggested by the Schlez & Infield is significantly different from the values proposed here and by Høvsøre model. This can due to the different time and length scale of the Schlez & Infield model, because its experiments were carried out using a distance between the points up to 100 m and a height above ground of 18 m.

Regarding the lateral decay factor, the comparison between the three models

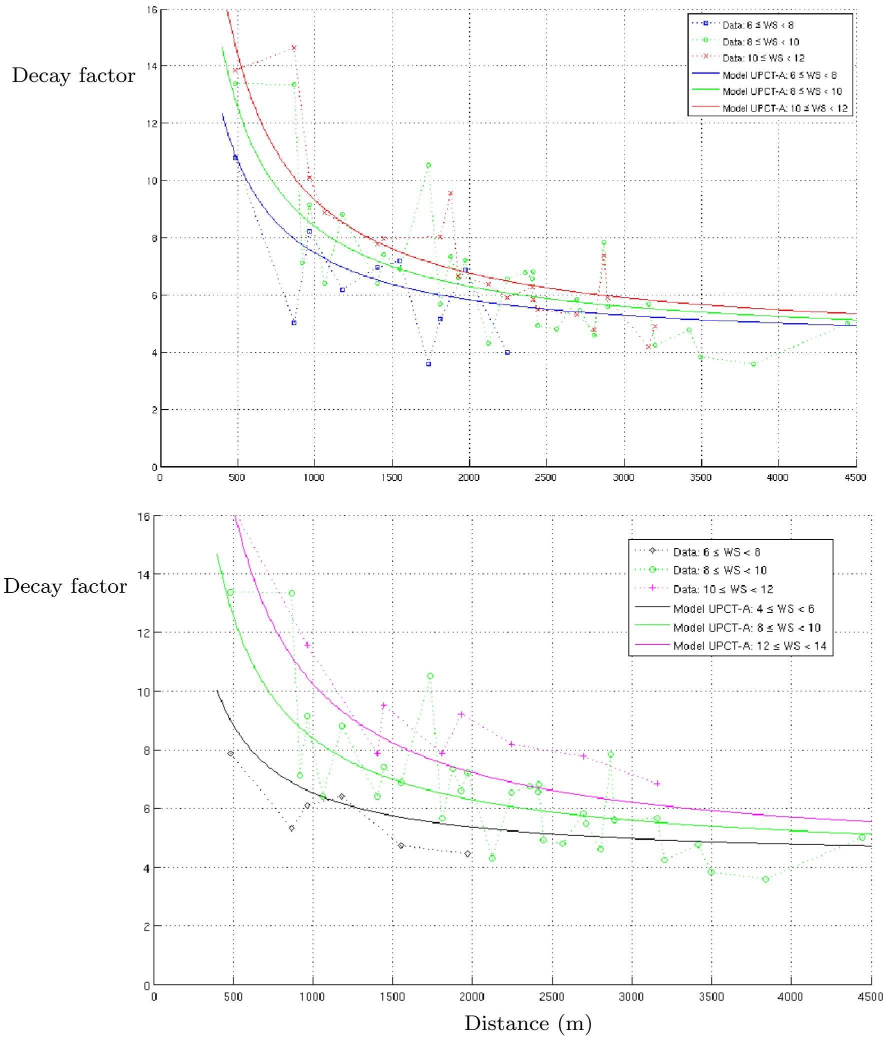

Figure 10. Comparison between the "measured" decay factors and the model UPCT-A in the lateral situation.

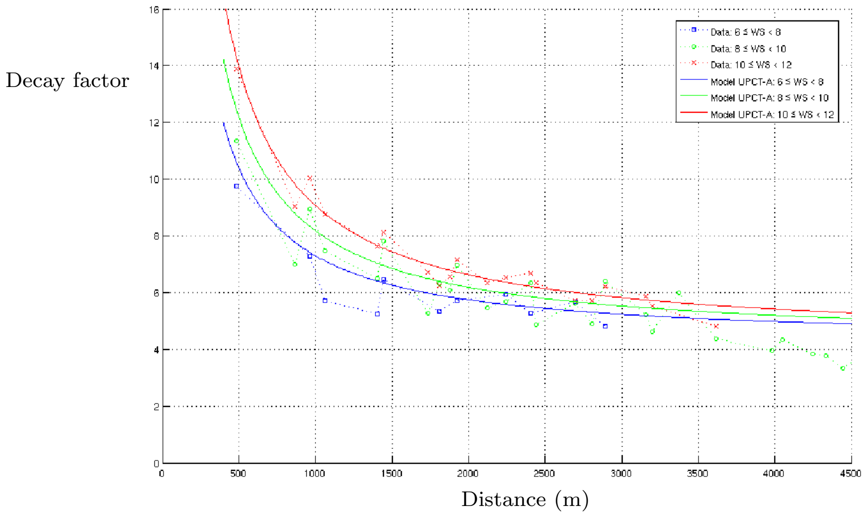

Figure 11. Comparison between the “measured” decay factors and the model UP-CT-A for inflow angles between 65 deg. and 84 deg.

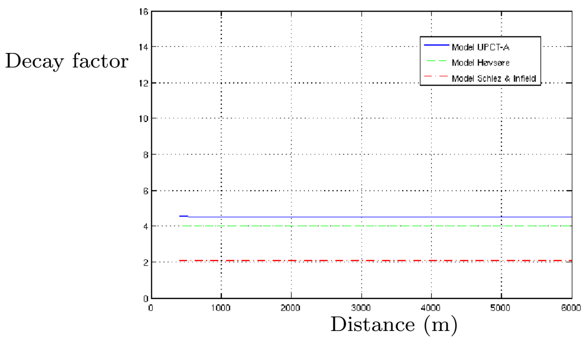

Figure 12. Comparison between the model UPCT-A, Høvsøre model and the Schlez& Infield model in the longitudinal situation.

can be found in figure 13. Schlez & Infield and Høvsøre model do not predict the distance dependence shown above. However, meanwhile Høvsøre predicts decay factors that are close to the model here presented for medium-high wind speeds and distances greater than 3 km., Schlez & Infield overestimates clearly the decay parameters in all the investigated distances, specially when rising the wind speed, which makes the predicted decay factor really huge. This overestimation would lead to an underestimation of the power fluctuations, if that model is used in this frame. Nevertheless, as it was expected if we consider a constant small distance, there is a qualitative agreement between the three models considering $a_{lat} \sim V$.

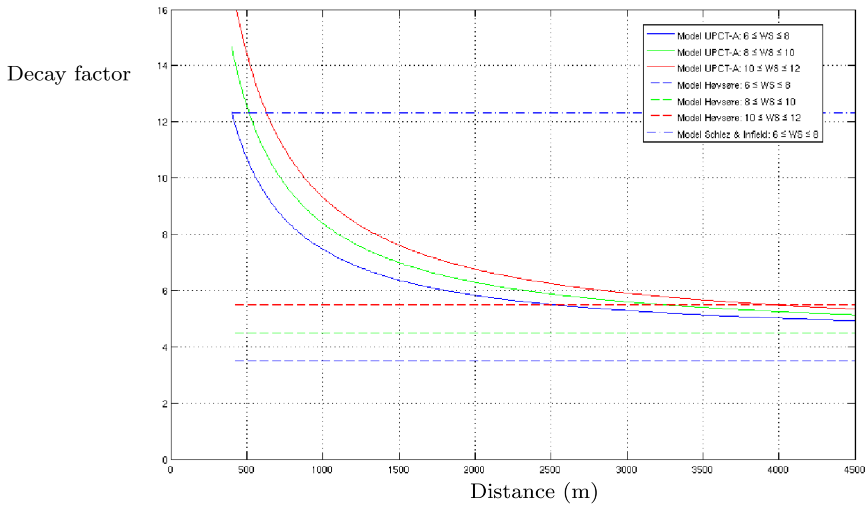

Figure 13. Comparison between the model UPCT-A, Høvsøre model and the Schlez& Infield model in the lateral situation.

8 Conclusions

Starting from 9 months of real data coming from a Large Offshore Wind Farm, it has been seen that there is a significant dependence between the coherence and the inflow angle, as in the model suggested by Schlez & Infield. However, it was also shown that in the length, height and time scale interesting for studying the power fluctuations of Large Wind Farms, the Schlez & Infield model predicts coherence values that are far from the experimental data shown here.

In those experimental data is shown that whereas the longitudinal situation can be modelled by means of a constant decay factor, there is a strong dependency between the decay factor in the lateral situation and the distance and wind speed.

From those differences, a model for the coherence has been developed. That model provides the spectral coherence between wind speeds located in a horizontal plane corresponding to hub height of wind turbines in a large wind farm. For the shake of simplicity, a reduced model is also provided.

That empirical model has been fitted in a time scale up to 2 hours and with distances from near 500 m to 6 km. The election of the scale, based in the bibliography above cited, makes this model suitable in the frame of Power Fluctuation.

The influence of the turbulent intensity has been analysed, suggesting a model that includes that parameter, however it is shown that its influence is not that important.

This coherence model can be used for improving power fluctuation simulations in offshore wind farms and even for evaluating the shape of large wind farms from this point of view.

Wake and other effects can be introduced for instance as it was described in several works (Sørensen et al., 2002; Frandsen, 2005; Sørensen et al., to appear).

9 Acknowledgements

The work presented in this paper has been done in the research project "Power Fluctuations from large offshore wind farms" financed by the Danish Transmission System Operator Energinet.dk as PSO 2004 project number 6506.

A. Vigueras-Rodríguez is supported by the Spanish Ministerio de Educación y Ciencia through the grant program "Becas FPU".

References

Akhmatov, V., Kjaergaard, J. P. and Abildgaard, H., 2004. Announcement of the large offshore wind farm Horns Rev B and experience from prior projects in Denmark, in: European Wind Energy Conference.

Davenport, A. G., 1961. The spectrum of horizontal gustiness near the ground in high winds. *Quarterly Journal of Meteorology Society* **87**, 194–211.

Frandsen, S., 2005. Turbulence and turbulence-generated structural loading in wind turbine clusters, Technical report, Risø National Laboratory.

Nanahara, T., Asari, M., Sato, T., Yamaguchi, K., Shibata, M. and Maejima, T., 2004. Smoothing effects of distributed wind turbines. Part 1. Coherence and smoothing effects at a wind farm. *Wind Energy* **7**, 61–74.

Schlez, W. and Infield, D., 1998. Horizontal, two point coherence for separations greater than the measurement height. *Boundary-Layer Meteorology* **87**, 459–480.

Solari, G., 1987. Turbulence modeling for gust loading. *ASCE Journal of Structural Engineering* **113**, 1550–1569.

Sørensen, P., Cutululis, N., Vigueras-Rodríguez, A., Madsen, H., Pinson, P., Jensen, L., Hjerrild, J. and Donovan, M., to appear. Modelling of power fluctuations from large offshore wind farms. *Wind Energy* .

Sørensen, P., Cutululis, N. A., Lund, T., Hansen, A. D., Sørensen, T., Hjerrild, J., Donovan, M. H., Christensen, L. and Nielsen, H. K., 2007. Power quality issues on wind power installations in Denmark, in: IEEE Power Engineering Society, General Meeting, Tampa, Florida, USA.

Sørensen, P., Hansen, A. D. and Rosas, P. E. C., 2002. Wind models for simulation of power fluctuations from wind farms. *Journal of Wind Engineering and Industrial Aerodynamics* **90**, 1381–1402.

Vigueras-Rodríguez, A., Sørensen, P. and Viedma, A., 2006. Spectral coherence models for the wind speed in large wind farms, in: Proceedings of the 2nd PhD Seminar on Wind Energy in Europe, European Academy of Wind Energy, Roskilde (Denmark).